Semiconducting CuO Nanotubes: Synthesis, Characterization, and Bifunctional Photocathodic Enzymatic Bioanalysis

Ling Zhang, Yuan-Cheng Zhu, Yan Yu Liang, Wei-Wei Zhao, Jing-Juan Xu, and Hong-Yuan Chen

Anal. Chem., **Just Accepted Manuscript** • DOI: 10.1021/acs.analchem.8b00742 • Publication Date (Web): 02 Apr 2018

Semiconducting CuO Nanotubes: Synthesis, Characterization, and Bi-functional Photocathodic Enzymatic Bioanalysis

Ling Zhang[1,2,3,5], Yuan-Cheng Zhu[2,5], Yan-Yu Liang[1,*], Wei-Wei Zhao[2,4,*], Jing-Juan Xu[2] and Hong-Yuan Chen[2]

[1]School of Materials Science and Technology, Nanjing University of Aeronautics and Astronautics, Nanjing 211106, China
[2]State Key Laboratory of Analytical Chemistry for Life Science and Collaborative Innovation Center of Chemistry for Life Science, School of Chemistry and Chemical Engineering, Nanjing University, Nanjing 210023, China
[3]School of Material and Chemical Engineering, Bengbu University, Bengbu 233000, China
[4]Department of Materials Science and Engineering, Stanford University, Stanford, California 94305, United States
[5]These authors (L. Z. and Y.-C. Z.) contributed to this work equally.
* E-mail: liangyy403@126.com * E-mail: zww@nju.edu.cn; zww@stanford.edu

ABSTRACT: This work reports the synthesis, characterization and application of bifunctional semiconducting CuO nanotubes (NTs) electrode for innovative synergized cathodic photoelectrochemical (PEC) enzymatic bioanalysis. Specifically, CuO NTs electrode was fabricated by surface oxidation of the copper foil in an alkaline aqueous solution with $(NH_4)_2S_2O_8$ and then annealed in air at 200 ºC. After the subsequent coupling with the model enzyme of xanthine oxidase (XOD), the resulted photocathodic enzyme biosensor exhibited good analytical performance of rapid response, high stability, and good sensitivity. Especially, due to the unique catalytic property of CuO toward H_2O_2, a novel enzymatic cascade design between biological catalyst (XOD as natural enzyme) and biomimetic catalyst (CuO as the peroxidase mimetics) was constructed, and the dual-catalyst system with special synergy effect could achieve the cathodic PEC guanine bioanalysis with enhanced efficiency. In the determination, the cathodic photocurrent was found to be proportional to the guanine concentration, which was different from the commonly observed O_2-dependent suppression of the photocurrent. In all, such a bifunctional CuO NTs based PEC bioassay format has not been reported. The success of this work can offer great chances for further development and implementation of novel CuO-based PEC bioanalytical systems. More importantly, the strategy proposed here could contribute to the development of an original prototype for general PEC enzymatic bioanalysis.

Cupric oxide (CuO), a p-type narrow-band-gap semiconductor and also an antiferromagnetic material, has been received extensive investigations for its wide applications in high-Tc superconductors,[1] gas sensors,[2] solar cells,[3] FE emitters,[4] electronic cathode materials,[5] lithium−copper oxide cells,[6] CO_2 electrochemical reduction,[7] and etc. As demonstrated that the important roles of morphologies in determining the performance of nanomaterials, CuO has also been processed into various nanostructures, such as nanoparticles (NPs),[8] nanotubes (NTs),[9] nanowires (NWs),[10] nanoneedles (NLs) , [11] nanorods (NRs)[12] and nanobelts (NBs),[13] for enhancing its performance in currently existing applications. Among them, one-dimensional (1-D) CuO nanomaterials are currently being investigated in great detail for their unique properties and versatile implementation.[14] For example, highly dense CuO NWs were grown by oxidation of Cu mesh in air and then reduced for low-overpotential CO_2 reduction.[7]

Natural enzymes can catalyze chemical reactions with high efficiency and specificity under mild and eco-friendly conditions,[15-19] whereas artificial enzyme mimetics possess the advantages of easy preparation, low cost, good stability/reusability, and high practicability under extreme conditions.[20-21] Nowadays, a variety of enzyme mimetics have been exploited, especialy the nanomaterials-based enzyme mimetics.[22] Among them, CuO nanomaterials have been widely investigated for use as a powerful heterogeneous catalyst for many purposes. For example, CuO NPs have been applied as an efficient and recyclable catalyst for cross-coupling reactions of organic diselenides with aryl boronic acids.[23] Ce-incorporated CuO_x has led to greatly improved oxygen evolution reaction (OER) activity.[24] Pd NPs-modified CuO nanorods have demonstrated as high performance electrocatalysts for glucose detection.[25] Particularly, CuO possesses efficient peroxidase-like activity that can catalyze H_2O_2 to initiate numbers of oxidations. For example, to study the peroxidase-like activity of the CuO NPs, the catalytic oxidation of the peroxidase substrate 3,3,5,5-tetramethylbenzidine (TMB) in the presence of H_2O_2 had been reported.[26] Water-soluble CuO NPs, with higher affinity to H_2O_2 than commercial CuO NPs, had also been fabricated for detection of H_2O_2 and glucose.[27] Various CuO based nanomaterials had also been exploited for many bioanalytical applications such as fluorometric assay[28] and colorimetric detection.[29]

Photoelectrochemical (PEC) bioanalysis has of growing interest due to its desirable properties and attractive potential in future bioanalysis.[30-38] Using p-type semiconductors, photocathodic bioanalysis represents a newly emerged direction of novel PEC bioanalysis and has of soaring interest over the recent years due to

its better performance as compared with the photoanodic bioanalysis.[39-40] Specifically, the special advantage of photocathodic bioanalysis is its good anti-interference capability against reductive substances. To date, despite their fascinating features, the research in this field lags far behind the photoanodic one, and only a paucity of photocathodic bioanalysis has been reported.[41-42] Given the p-type semiconductor behavior of CuO and its intrinsic catalytic activity, some questions then naturally arise at this point: (i) whether CuO could be implemented in a proper nanosystem to function both as photocathode and biomimetic catalyst? (ii) could CuO act as an ideal platform to accommodate natural enzyme and then cooperate with the enzyme to form a coupled catalytic cascade? (iii) what will be the impact of the possible synergy effect on the performance of the resultant PEC biosensor? However, to date no effort has been devoted to shed light on such a possibility.

With these motivations, here we report the CuO NTs-based cascade-type reaction for elegant photocathodic bioanalysis of guanine, exemplified by xanthine oxidase (XOD) as a model biocatalyst. Specifically, As shown in Scheme 1, CuO NTs electrode was initially fabricated by preparation of $Cu(OH)_2$ NTs on the Cu foil via a mild, template-free, aqueous route and then the CuO NTs was in situ formed by transformation of the $Cu(OH)_2$ NTs to CuO NTs through a heat treatment process.[43] After the enzyme assembly, the as-obtained biosensor was tested for the guanine determination, during which the cathodic photocurrent was found to be proportional to the guanine concentration, which was different from the commonly observed O_2-dependent suppression of the photocurrent. This phenomenon was due to the synergy between the XOD-induced biocatalytic event and the CuO caused nanocatalytic process. According to a recent review about PEC enzymatic biosensors,[44] such a bifunctional CuO NTs based PEC bioassay format and the corresponding mechanism has not been reported. The success of this work can offer great chances for further development and implementation of novel CuO-based PEC bioanalytical systems. More importantly, the strategy proposed here would develop into the embryonic form of an original prototype for a general PEC bioanalysis. The detailed characterization, performance characteristics, and especially, the mechanism discussion of the biosensor are presented thereinafter.

Scheme 1. The Proposed Biofunctional CuO NTs-Based Photocathodic Bioanalysis

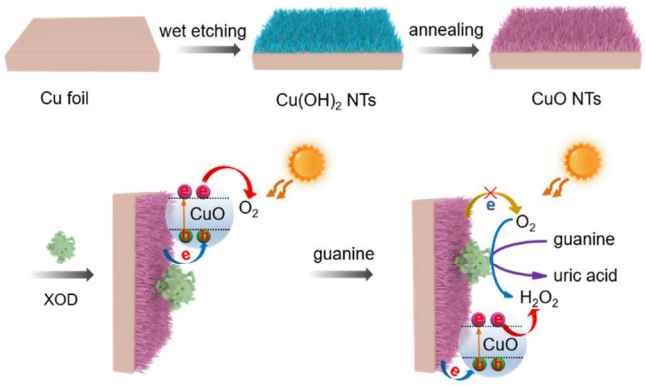

EXPERIMENTAL SECTION

Chemicals and Materials. XOD (5 UN), dopamine (DA), N-(3-dimethylaminopropyl)-N-ethyl-carbodiimide Poly (diallyldimethylammonium chloride) (PDDA, 20%, w/w in water, MW = 200 000-350 000) were supplied from Sigma-Aldrich, (St. Louis, MO). Guanine, ascorbic acid (AA), HCl, KCl, NaCl, L-phenylalanine, L-histidine, Tris (hydroxymethyl) aminomethane (Tris), copper foil (0.1mm), sodium hydroxide, ammonium persulphate were supplied from Sinopharm Chemical Reagent Co., Ltd (China). All other chemicals used were analytical grade. Ultrapure water (18.2 MΩ·cm resistivity at 25 °C, Milli-Q) was used in all experiments.

Instrumentation. Scanning electron microscope (SEM) images were recorded by a Hitachi S4800 scanning electron microscope (Hitachi Co., Japan). Transmission electron microscope (TEM) was performed with a JEM-2100 microscope (JEOL, Japan). X-ray photoelectron spectroscopy (XPS) was obtained from PHI 5000 VersaProbe (UlVAC-PHI Co., Japan). UV−vis diffuse reflectance spectra were obtained on a Shimadzu UV-3600 UV-vis-NIR spectrophotometer (Shimadzu Co., Japan). The crystallographic and purity information of the samples were characterized by powder X-ray diffraction (XRD, X'TRA, Cu Kα; ARL Co., Switzerland).

PEC measurements were performed using a homemade PEC system equipped with a 5 W LED lamp emitting at around 410nm with a power density of 1.6 mW cm^{-2}. Photocurrent was measured on a CHI 660C electrochemical workstation with three-electrode system: a CuO NTs/ITO electrode with a geometrical circular area (0.5 cm in diameter) as the working electrode, a Pt wire as the counter electrode and a saturated Ag/AgCl electrode as the reference electrode. The photocurrent measurements were performed at a constant potential of 0.0 V (vs saturated Ag/AgCl). A 0.01 M Tris–HCl (pH 7.4) was used as the supporting electrolyte for photocurrent measurements.

Preparation of CuO NTs. The synthesis of CuO NTs on the copper substrate was performed as follows. Firstly, $Cu(OH)_2$ NTs were fabricated on the Cu foil by surface chemical oxidation in an alkaline medium at room temprerature according to a previous report[45] with modifications. Typically, After sonicated in a solution of ethanol and acetone for 5 min followed by Milli-Q for 5 min to remove the organic contaminants, the Cu foil (3 cm×0.7 cm) was immersed in the solution of 2.67 M NaOH and 0.13 M $(NH_4)_2S_2O_8$. With the surface covered with a deep-blue film, the piece of copper was taken out from the solution and rinsed with distilled water thoroughly. After dried with N_2, the fabricated $Cu(OH)_2$ NTs/Cu electrode was put into the center of a quartz tube and thermally annealed in air at 200 ℃ for 1h. Finally the sample was cooled to room temperature and a black layer of CuO NTs were formed on the surface of the Cu foil.

Development of Enzyme biosensor. The fabricated CuO NTs/Cu electrodes were activated by casting 10 μL 2% PDDA containing 0.5 M NaCl for 30 min. Followed by thoroughly rising with water, 10 μL 0.5 mg/mL XOD was added onto the CuO NTs/Cu electrode for the conjugation of XOD to the adhered PDDA. After incubated at room temperature for another 30 min, a monolayer of XOD was modified on the combined electrodes. Repeating the process of casting PDDA and XOD solution, multilayers of XOD modified electrodes could be accepted. And the resulting XOD conjugated CuO NTs/Cu electrodes were stored at 4 °C for use. For the detection of guanine, the XOD modified CuO NTs/Cu electrodes were immersed into the 7 ml 0.01 M Tris-HCl buffer (pH=7.4) containing certain concentration of guanine at 35 °C. And the photocurrents of the CuO NTs/Cu electrodes were measured 20 minutes later.

RESULTS AND DISCUSSION

Materials Characterizations. The morphologies of the as-prepared samples were displayed by SEM and TEM. As shown in

Figure 1a, the SEM image of $Cu(OH)_2$ demonstrates the formation of $Cu(OH)_2$ in wire-like structure directly on the Cu surface, whereas the clear open structures (arrows in figure 1a) of the wire tips reveal the tubular structure of theses wires, which are near circular with the diameters in the range of 100-250 nm. As shown in Figure 1a inset, the high-resolution SEM reveals the uneven and irregular tip opening of $Cu(OH)_2$ NTs more clearly. In order to further present the structural information of $Cu(OH)_2$ NTs, the sample was removed from the Cu foil for TEM determination. As shown in Figure 1b, the $Cu(OH)_2$ NTs possessed a relative smooth surface and uniform diameters range from 100 to 250 nm, which were consistent with the SEM images. Upon further magnification, as shown in Figure 1b inset of the HR-TEM image, a lattice fringe of 0.263 nm was determined, corresponding well to the (002) facet of $Cu(OH)_2$. The $Cu(OH)_2$ NTs were transformed to CuO NTs by the annealing process. As shown in Figure 1c, the SEM image reveals the CuO NTs with the diameter ranged from 50 to 250 nm, which were more bending than $Cu(OH)_2$ NTs. Besides, the surface of the CuO NTs was not as smooth as that of $Cu(OH)_2$ NTs, which may be result from the stacking of the nanoparticles during the annealing. As shown in Figure 1c inset, the higher magnification image confirmed that the CuO NTs had kept the tubular structure. In addition, the morphology of CuO NTs was further recorded by TEM observations. As shown in Figure 1d, similar dimensions and the rough surface were recorded, which were in good accordance with the results of the SEM. Furthermore, as shown in Figure 1d inset, a clear interfacial lattice spacing of 0.252 nm can be ascribed to the (002) facet of CuO. Obviously, such a nanoporous structure would be advantageous for the immobilization of biomolecules.

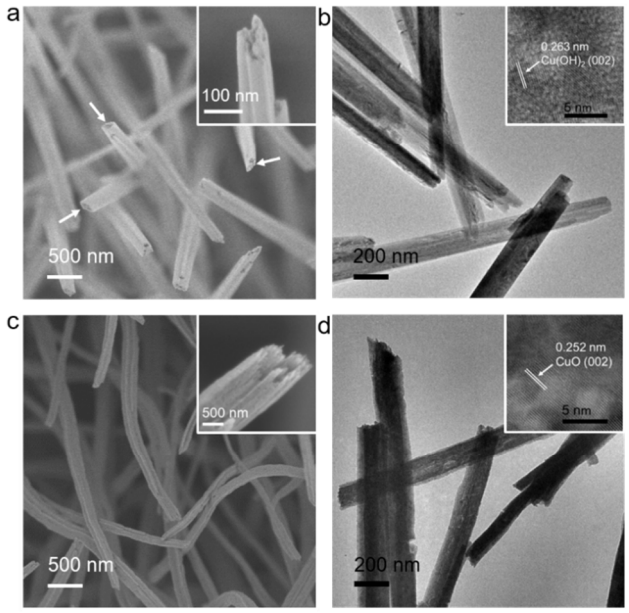

Figure 1. (a) SEM and HR-SEM (inset) images of the $Cu(OH)_2$ NTs/Cu electrode. (b) TEM and HR-TEM (inset) images of $Cu(OH)_2$ NTs. (c) SEM and HR-SEM (inset) images of the CuO NTs/Cu electrode. (d) TEM and HR-TEM (Inset) images of the CuO NTs.

The crystal structures of the as-prepared samples on the Cu substrate were then identified by XRD. As shown in Figure 2a, quantitative analysis of the pattern for $Cu(OH)_2$ would index all the observed peaks to the orthorhombic $Cu(OH)_2$ phase, except those peaks of Cu. Compared with the standard diffraction pattern (JCPDS No. 13-0420), no related impurity existed in the sample. Therefore, pure $Cu(OH)_2$ NTs have been successfully grown on the Cu foil. After heat treatment in air, the structure of $Cu(OH)_2$ NTs would rapidly be damaged due to the transformation from $Cu(OH)_2$ to nanocrystallites of CuO. By calcining at 200 □, the XRD pattern of the as-prepared sample on the Cu surface shows that the diffraction peaks displayed at 35.5° and 38.7° were in corresponding to the (002), (111) plans of monoclinic CuO phase (JCPDS No.45-0937). In addition to the strong peaks of copper, no other diffraction peak can be found. But with the calcining temperature increase to 250 □ and 300 □, diffraction peaks of Cu_2O would appear (JCPDS No.05-0667), which may be formed from the surface oxidation of Cu foil during the annealing process. 200 □ was thus chose as the final calcining temperature to transform $Cu(OH)_2$ NTs/Cu electrode to pure CuO NTs/Cu electrode.

The surface chemical composition was characterized using the XPS, and all the XPS data were calibrated by the carbon 1s peak at 284.6 eV. As shown in Figure 2b, the whole survey of the proposed electrode surface presented all the elements detected, indicating that there was no other related impurity existing in the sample. Figure 2b inset displays two peaks positioned at 933.7 eV and 953.6 eV, which can be ascribe to Cu $_{2p3/2}$ and Cu $_{2p1/2}$ in CuO.[46,47] The rest of the shakeup satellite peaks positioned at 943.6 and 962.2 eV were ~ 9 eV higher banding energy compared to the main peaks, which further confirms the existence of Cu(II) in the fabricated sample.[48] The XPS result, together with the XRD result, confirmed that the $Cu(OH)_2$ NTs have been completely converted to CuO NTs.

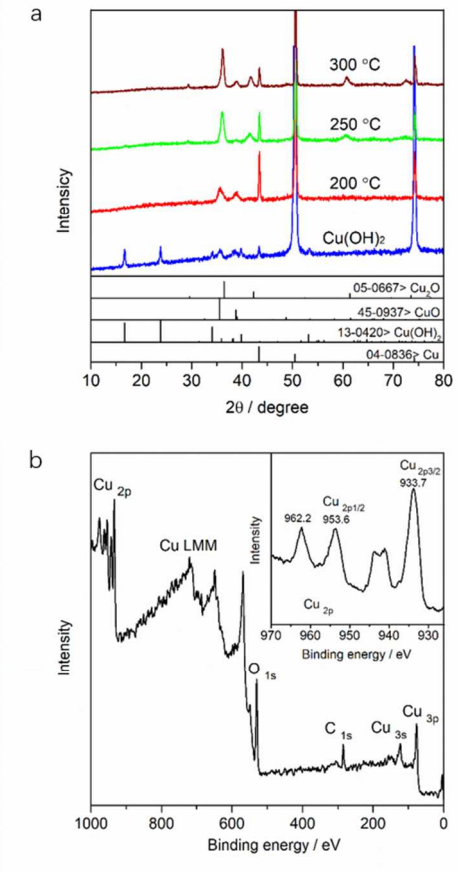

Figure 2. (a) XRD patterns of the as-fabricated $Cu(OH)_2$ NTs/Cu electrode before and after annealing at different temperatures. (b) The full-scan XPS spectrum of the as-fabricated CuO NTs/Cu electrode and the high-resolution XPS spectra of Cu $_{2p}$ (inset).

The optical property of the photoelectrode was investigated by DRS. As shown in Figure 3a, it could be observed that the light absorption edge of CuO NTs started at 865 nm. As a crystalline semiconductor, the relationship of band edge and optical absorption can be determined by the equation:

$$\alpha h\nu = A(h\nu - E_g)^{n/2}$$

where hν, α, E_g and A represent the photon energy, optical absorption coefficient, band gap, and proportionality constant, respectively.[49] Because the optical transitions of CuO are direct,[50] the band gap energies of all the NTs can be estimated from the plots of $(\alpha h\nu)^2$ versus photon energy (hν). As shown in Figure 3b, the intercept of the tangent to the X axis would give a good approximation of the band gap energies of 1.98 eV for the fabricated sample, which was in good agreement with earlier reports of the band gap of bulk copper oxide (1.2-2.1 eV).[14, 51]

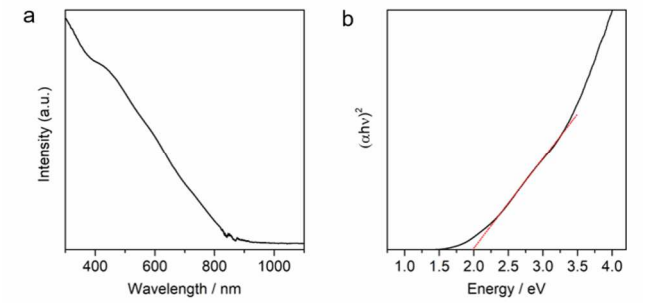

Figure 3. (a) UV-vis diffuse reflectance spectra of the fabricated CuO NTs/Cu electrode. (b) Plot of $(\alpha h\nu)^2$ versus energy (hν).

PEC Characterization. Compared with the widely used TiO_2 NTs, CuO NTs have a broad absorption spectrum in the visible to near infrared range, which can produce multiple charge carriers after absorbing a photon and lead to higher photo-to-electron output.[52] As shown in Figure 4a, as p-type semiconductor, the CuO NTs electrode produced a stable cathodic photocurrent. The operational stability of the photocurrent response of CuO NTs electrode upon repeated on/off illumination cycles over 5 min had also been revealed. The corresponding photocurrent generation mechanism of the electrode was displayed in Scheme 1. Under illumination, the photogenerated electrons and holes would formed on the conduction band (CB) and valence band (VB) of CuO NTs, respectively. With the photogenerated electrons transferred from the CB of CuO to the electron acceptors (the dissolved oxygen) in the electrolyte and photogenerated holes captured by the electrons of the Cu electrode, a stable cathodic photocurrent can be generated. The reproducible responses without any noticeable decrease indicate the high mechanical and photophysical stability of the electrode in PEC measurements. Besides, Figure 4b reveals that the cathodic photocurrent intensity upon illumination (solid line) and in the dark (dashed line) increased with the application of cathodic bias. Considering the higher bias is harm to biological samples, 0.0 v vs Ag/AgCl was used as the working voltage. In order to study the sensitivity of CuO photocathode to ambient O_2, highly pure nitrogen (N_2) was purged to deoxygenate the solution. As shown in Figure 4c, the photocurrent responses go down gradually with the increase of nitrogen-purged time, which demonstrates the fabricated electrodes are oxygen-sensitive. Once the dissolved oxygen amount decreased with the N_2 purging, the cathodic photocurrents will be inhabinated result from the increased electron-hole pairs recombination of the CuO NTs. Incidentally, the photocurrent responses of the proposed CuO NTs electrodes versus the alkaline chemical bath time of Cu foils was optimized with the results in Figure 4d. the photocurrents enhanced with the increase of the reaction time and reached the maximum within 15 min. Whereafter, a decrease tendency of the cathodic photocurrents appeared due to the increment of the barrier effect for the diffusion of dissolved oxygen to the inner portion of the CuO NTs. So 15 min was chosen as the wet etching time so as to get the optimal PEC performance of the photocathode.

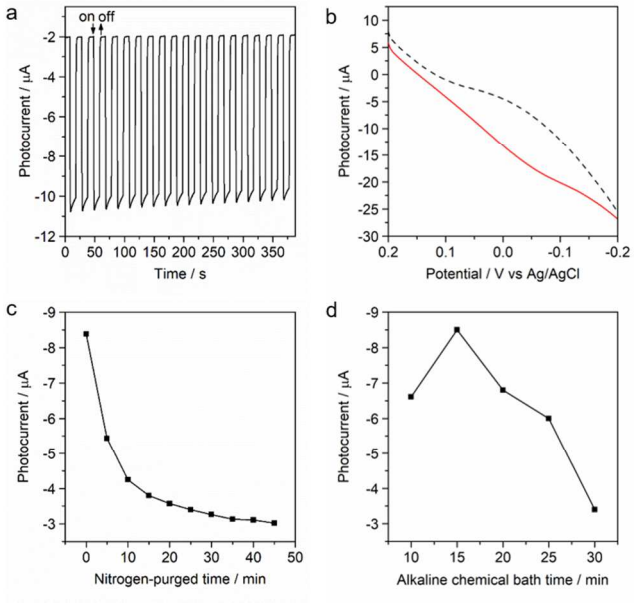

Figure 4. (a) The operational stability test of the as-fabricated CuO NTs/Cu electrode by repeated on/off illumination cycles. (b) I–V characteristic curves of the electrode upon illumination (solid line) and in the dark (dashed line) with the range of +0.2 to -0.2 V. (c) Photocurrent responses of CuO NTs/Cu electrode to the time of purging nitrogen to wipe off oxygen in a 0.01 M Tris-HCl solution (pH=7.4) at 0.0 V vs. Ag/AgCl under a 410 nm light excitation. (d) Effect of the alkaline chemical bath deposited time on the photocurrent responses of the CuO NTs/Cu electrodes.

Analytical Performance. The as-developed CuO NTs photocathode was then coupled with XOD and applied for guanine detection. Figure 5a demonstrates the stepwise photocurrent responses along with the biosensor development. As shown, upon illumination, the CuO NTs electrode exhibited significant cathodic photocurrent (black curve) under no biased potential. After the loading of enzyme, as expected, obvious reduction of signal intensity was observed (red curve), which could be ascribed to the insulating effect of the protein molecules that inhibited the interfacial electron transfer.[53-54] When in the presence of 50 μM guanine, we observed an enhanced photocurrent signal (blue curve), rather than the common O_2-dependent suppression of the signal in conventional PEC enzymatic biosensors. This phenomenon confirmed the recently proposed dual-catalysis mechanism,[55] the effect of the natural oxidase of XOD synergized with the biomimetic catalyst of CuO NTs. The peroxidase property of CuO NTs was easily revealed by the use of H_2O_2 solution. As demonstrated in Figure 5b, the cathodic signal intensity enhanced rapidly with the increase of H_2O_2 concentration. As expected and shown in Figure 5c, the cathodic photocurrent intensity enhanced with the increased guanine concentration, which would introduce H_2O_2 to control the signal intensity. The corresponding derived calibration curve in Figure 5c inset demonstrates a good linear relation-

ship between the percentage of the photocurrent increase and the logarithm of the guanine concentrations in the range from 0.1μM to 50 μM, with a detection limit of 0.04 μM (S/N = 3). The analytical performance of this PEC biosensor for the detection of guanine was comparable to some recent reports.[56,57] In addition, the high accessibility and low cost of this protocol makes it a promising platform for many other analytes of interest. By assaying 0.01 mM guanine with five sensors prepared at the same experiment conditions, the relative standard deviation (RSD) was calculated to be 6.9%, indicating the satisfactory precision and reproducibility of this PEC enzymatic bioanalysis. In addition, to reveal the selectivity, control experiments were performed. The photocurrent responses of the XOD modified photoelectrodes to several kinds of amino acids, inorganic salts, ascorbic acid and dopamine in the same conditions had been presented in Figure 5d. As shown, these interfering substances had no obvious effect on the detection of guanine at the same concentration of 0.01 mM. The good selectivity should be ascribed to the inherent specificity of enzyme and the use of cathodic photoelectrode system which has good anti-interference capability against reductive substances.[41]

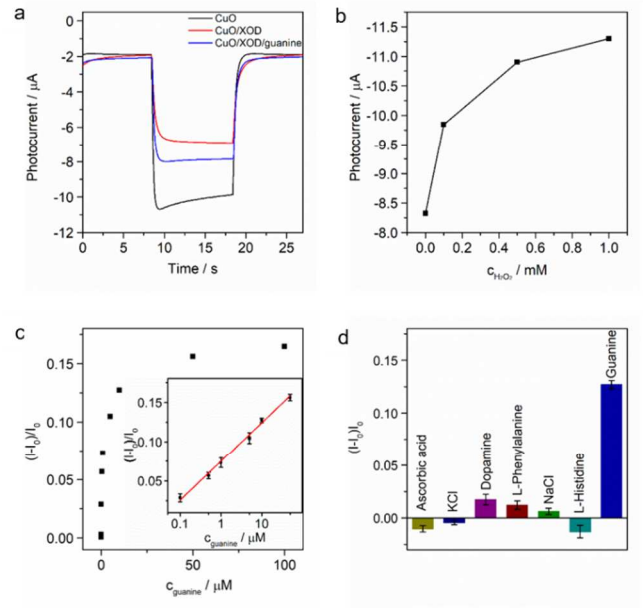

Figure 5. (a) Photocurrent responses of CuO NTs/Cu electrode before (dark curve) and after (red curve) XOD modification corresponding to air saturated 0.01 M Tris-HCl solution (pH=7.4) without and with (blue curve) the addition of 50 μM guanine. (b) Photocurrent responses of CuO NTs/Cu electrodes in air-saturated Tris-HCl solution (pH 7.4) containing different concentrations of H_2O_2 (0, 0.1, 0.5, 1 mM). (c) Photocurrent responses of guanine with different concentrations and the corresponding calibration curve (Inset). (d) Effect of 0.01 mM different substances on the photocurrent responses of the enzyme modified electrodes. I_0 and I were the photocurrents of enzyme modified electrode before and after reaction with different substances, respectively. The PEC tests were performed with 0.0V applied voltage vs. Ag/AgCl and a 410 nm excitation light.

CONCLUSIONS

In this work, CuO NTs electrodes were fabricated, characterized and applied as bifunctional photocathode for innovative PEC enzymatic bioanalysis. The CuO NTs electrodes acted not only as the p-type semiconductor to generate the cathodic photocurrent signal, but also as the biomimetic catalyst to synergize the biological catalyst XOD to constitute the dual-catalysis system. In the detection, the effect of the XOD was succeeded by that of the CuO, i.e. the enzymatic product of H_2O_2 was catalyzed by the CuO promptly, resulting in the H_2O_2-controlled increase of the cathodic photocurrent rather than the O_2-controlled decrease of the signal. In all, such a CuO NTs-based photocathodic enzymatic bioanalysis has not been reported, the proposed photoelectrode may serve as a common basis for other PEC bioanalytical applications and stimulate the exploitation of numerous other bifunctional nanostructured semiconductors. Besides, the mechanism disclosed here also enriched the perspectives for the utilization of various photoactive enzyme mimetics in future PEC bioanalysis.

AUTHOR INFORMATION

Corresponding Author

* E-mail: liangyy403@126.com
* E-mail: zww@nju.edu.cn; zww@stanford.edu

Author contributions

L.Z. and Y.-C.Z. contributed equally.

Notes

The authors declare no competing financial interest.

ACKNOWLEDGMENT

We thank the National Natural Science Foundation of China (Grant Nos. 21327902 , 21675080 and 21771107), Natural Science Foundation of Jiangsu Province (Grant Nos. BK20161484, BK20170073), and the Fundamental Research Funds for the Central Universities (Grant NO. NE2015003). This work was also supported by a Project Funded by the Priority Academic Program Development of Jiangsu Higher Education Institutions.

REFERENCE

(1) Kimura, T.; Sekio, Y.; Nakamura, H.; Siegrist, T.; Ramirez, A. P. Cupric oxide as an induced-multiferroic with high-T-C. *Nat. Mater.* **2008,** *7,* 291-294.

(2) Lupan, O.; Cretu, V.; Postica, V.; Ababii, N.; Polonskyi, O.; Kaidas, V.; Schut, F.; Mishra, Y. K.; Monaico, E.; Tiginyanu, I.; Sontea, V.; Strunskus, T.; Faupel, F.; Adelung, R. Enhanced ethanol vapour sensing performances of copper oxide nanocrystals with mixed phases. *Sens. Actuators, B* **2016,** *224,* 434-448.

(3) Zuo, C. T.; Ding, L. M. Solution-processed Cu_2O and CuO as hole transport materials for efficient perovskite solar cells. *Small* **2015,** *11,* 5528-5532.

(4) Hsieh, C. T.; Chen, J. M.; Lin, H. H.; Shih, H. C. Field emission from various CuO nanostructures. *Appl. Phys. Lett.* **2003,** *83,* 3383-3385.

(5) Kushwaha, A.; Moakhar, R. S.; Goh, G. K. L.; Dalapati, G. K. Morphologically tailored CuO photocathode using aqueous solution technique for enhanced visible light driven water splitting. *Photochem. Photobiol., A* **2017,** *337,* 54-61.

(6) Hu, L.; Huang, Y.; Zhang, F.; Chen, Q. CuO/Cu_2O composite hollow polyhedrons fabricated from metal-organic framework templates for lithium-ion battery anodes with a long cycling life. *Nanoscale* **2013,** *5,* 4186-4190.

(7) Raciti, D.; Livi, K. J.; Wang, C. Highly dense Cu nanowires for low-overpotential CO_2 reduction. *Nano Lett.* **2015,** *15,* 6829-6835.

(8) Cronholm, P.; Karlsson, H. L.; Hedberg, J.; Lowe, T. A.; Winnberg, L.; Elihn, K.; Wallinder, I. O.; Moller, L. Intracellular uptake and toxicity of Ag and CuO nanoparticles: A comparison

between nanoparticles and their corresponding metal ions. *Small* **2013,** *9,* 970-982.
(9) Mu, C.; He, J. Confined conversion of CuS nanowires to CuO nanotubes by annealing-induced diffusion in nanochannels. *Nanoscale Res. Lett.* **2011,** *6,* 150.
(10) Jiang, X. C.; Herricks, T.; Xia, Y. N. CuO nanowires can be synthesized by heating copper substrates in air. *Nano Lett.* **2002,** *2,* 1333-1338.
(11) Rao, P. M.; Zheng, X. Rapid catalyst-free flame synthesis of dense, aligned α-Fe_2O_3 nanoflake and CuO nanoneedle arrays. *Nano Lett.* **2009,** *9,* 3001-3006.
(12) Liu, X.; Du, B.; Sun, Y.; Yu, M.; Yin, Y.; Tang, W.; Chen, C.; Sun, L.; Yang, B.; Cao, W.; Ashfold, M. N. R. Sensitive room temperature photoluminescence-based sensing of H_2S with novel CuO–ZnO nanorods. *ACS Appl. Mat. Interfaces* **2016,** *8,* 16379-16385.
(13) Zhang, X.; Yu, L.; Wang, L.; Ji, R.; Wang, G.; Geng, B. High electrochemical performance based on ultrathin porous CuO nanobelts grown on Cu substrate as integrated electrode. *PCCP* **2013,** *15,* 521-525.
(14) Zhang, Q.; Zhang, K.; Xu, D.; Yang, G.; Huang, H.; Nie, F.; Liu, C.; Yang, S. CuO nanostructures: Synthesis, characterization, growth mechanisms, fundamental properties, and applications. *Prog. Mater Sci.* **2014,** *60,* 208-337.
(15) Tang, J.; Li, J.; Da, P.; Wang, Y.; Zheng, G. Solar-energy-driven photoelectrochemical biosensing using TiO_2 nanowires. *Chem. Eur. J.* **2015,** *21,* 11288-11299.
(16) Shu, J.; Qiu, Z.; Lin, Z.; Cai, G.; Yang, H.; Tang, D. Semiautomated support photoelectrochemical immunosensing platform for portable and high-throughput immunoassay based on Au nanocrystal decorated specific crystal facets BiVO4 photoanode. *Anal. Chem.* **2016,** *88,* 12539-12546.
(17) Zeng, X.; Tu, W.; Li, J.; Bao, J.; Dai, Z. Photoelectrochemical biosensor using enzyme-catalyzed in situ propagation of CdS quantum dots on graphene oxide. *ACS Appl. Mat. Interfaces* **2014,** *6,* 16197-16203.
(18) An, Y.; Tang, L.; Jiang, X.; Chen, H.; Yang, M.; Jin, L.; Zhang, S.; Wang, C.; Zhang, W. A Photoelectrochemical immunosensor based on Au-doped TiO_2 nanotube arrays for the detection of alpha-synuclein. *Chem. Eur. J.* **2010,** *16,* 14439-14446.
(19) Zheng, Y. N.; Liang, W. B.; Xiong, C. Y.; Yuan, Y. L.; Chai, Y. Q.; Yuan, R. Self-enhanced ultrasensitive photoelectrochemical biosensor based on nanocapsule packaging both donor–acceptor-type photoactive material and its sensitizer. *Anal. Chem.* **2016,** *88,* 8698-8705.
(20) Li, L.; Ai, L.; Zhang, C.; Jiang, J. Hierarchical {001}-faceted BiOBr microspheres as a novel biomimetic catalyst: dark catalysis towards colorimetric biosensing and pollutant degradation. *Nanoscale* **2014,** *6,* 4627-4634.
(21) Gao, L.; Zhuang, J.; Nie, L.; Zhang, J.; Zhang, Y.; Gu, N.; Wang, T.; Feng, J.; Yang, D.; Perrett, S.; Yan, X. Intrinsic peroxidase-like activity of ferromagnetic nanoparticles. *Nat. Nanotechnol.* **2007,** *2,* 577-583.
(22) Wei, H.; Wang, E. Nanomaterials with enzyme-like characteristics (nanozymes): next-generation artificial enzymes. *Chem. Soc. Rev.* **2013,** *42,* 6060-6093.
(23) Alves, D.; Santos, C. G.; Paixao, M. W.; Soares, L. C.; de Souza, D.; Rodrigues, O. E. D.; Braga, A. L. CuO nanoparticles: an efficient and recyclable catalyst for cross-coupling reactions of organic diselenides with aryl boronic acids. *Tetrahedron Lett.* **2009,** *50,* 6635-6638.
(24) Chen, Z.; Kronawitter, C. X.; Yang, X.; Yeh, Y.-w.; Yao, N.; Koel, B. E. The promoting effect of tetravalent cerium on the oxygen evolution activity of copper oxide catalysts. *PCCP* **2017,** *19,* 31545-31552.
(25) Chen, Z.; Zhao, B.; Fu, X.-Z.; Sun, R.; Wong, C.-P. CuO nanorods supported Pd nanoparticles as high performance electrocatalysts for glucose detection. *J. Electroanal. Chem.* **2017,** *807,* 220-227.
(26) Chen, W.; Chen, J.; Liu, A.; Wang, L.; Li, G.; Lin, X. Peroxidase-like activity of cupric oxide nanoparticle. *ChemCatChem* **2011**, *3*, 1151-1154.
(27) Chen, W.; Chen, J.; Feng, Y.; Hong, L.; Chen, Q.; Wu, L.; Lin, X.; Xia, X. Peroxidase-like activity of water-soluble cupric oxide nanoparticles and ist analytical application for detection of hydrogen peroxide and glucose. *Analyst*, **2012**, *137*, 1706-1712.
(28) Hu, A. L.; Deng, H. H.; Zheng, X. Q.; Wu, Y. Y.; Lin, X. L.; Liu, A. L.; Xia, X. H.; Peng, H. P.; Chen, W.; Hong, G. L. Self-cascade reaction catalyzed by CuO nanoparticle-based dual-functional enzyme mimics. *Biosens. Bioelectron.* **2017,** *97,* 21-25.
(29) Zhang, L.; Hai, X.; Xia, C.; Chen, X.-W.; Wang, J.-H. Growth of CuO nanoneedles on graphene quantum dots as peroxidase mimics for sensitive colorimetric detection of hydrogen peroxide and glucose. *Sens. Actuators, B* **2017,** *248,* 374-384.
(30) Kang, Q.; Yang, L.; Chen, Y.; Luo, S.; Wen, L.; Cai, Q.; Yao, S. Photoelectrochemical detection of pentachlorophenol with a multiple hybrid CdSexTe1-x/TiO_2 nanotube structure-based label-free immunosensor. *Anal. Chem.* **2010,** *82,* 9749-9754.
(31) Li, L.; Zhang, Y.; Zhang, L.; Ge, S.; Liu, H.; Ren, N.; Yan, M.; Yu, J. Paper-based device for colorimetric and photoelectrochemical quantification of the flux of H_2O_2 releasing from MCF-7 cancer cells. *Anal. Chem.* **2016,** *88,* 5369-5377.
(32) Hao, N.; Zhang, X.; Zhou, Z.; Qian, J.; Liu, Q.; Chen, S.; Zhang, Y.; Wang, K. Three-dimensional nitrogen-doped graphene porous hydrogel fabricated biosensing platform with enhanced photoelectrochemical performance. *Sens. Actuators, B* **2017,** *250,* 476-483.
(33) Chen, D.; Zhang, H.; Li, X.; Li, J. Biofunctional titania nanotubes for visible-light-activated photoelectrochemical biosensing. *Anal. Chem.* **2010,** *82,* 2253-2261.
(34) Li, C.; Wang, H.; Shen, J.; Tang, B. Cyclometalated iridium complex-based label-free photoelectrochemical biosensor for DNA detection by hybridization chain reaction amplification. *Anal. Chem.* **2015,** *87,* 4283-4291.
(35) Long, Y.-T.; Kong, C.; Li, D.-W.; Li, Y.; Chowdhury, S.; Tian, H. Ultrasensitive determination of cysteine based on the photocurrent of nafion-functionalized CdS-MV quantum dots on an ITO electrode. *Small* **2011,** *7,* 1624-1628.
(36) Li, H.; Mu, Y.; Yan, J.; Cui, D.; Ou, W.; Wan, Y.; Liu, S. Label-free photoelectrochemical immunosensor for neutrophil gelatinase-associated lipocalin based on the use of nanobodies. *Anal. Chem.* **2015,** *87,* 2007-2015.
(37) Yan, K.; Liu, Y.; Yang, Y.; Zhang, J. A cathodic "signal-off" photoelectrochemical aptasensor for ultrasensitive and selective detection of oxytetracycline. *Anal. Chem.* **2015,** *87,* 12215-12220.
(38) Li, R.; Yan, R.; Bao, J.; Tu, W.; Dai, Z. A localized surface plasmon resonance-enhanced photoelectrochemical biosensing strategy for highly sensitive and scatheless cell assay under red light excitation. *Chem. Commun.* **2016,** *52,* 11799-11802.
(39) Zhang, X.; Liu, M.; Liu, H.; Zhang, S. Low-toxic Ag2S quantum dots for photoelectrochemical detection glucose and cancer cells. *Biosens. Bioelectron.* **2014,** *56,* 307-312.
(40) Tanne, J.; Schäfer, D.; Khalid, W.; Parak, W. J.; Lisdat, F. Light-controlled bioelectrochemical sensor based on CdSe/ZnS quantum dots. *Anal. Chem.* **2011,** *83,* 7778-7785.
(41) Wang, G. L.; Shu, J. X.; Dong, Y. M.; Wu, X. M.; Zhao, W. W.; Xu, J. J.; Chen, H. Y. Using G-Quadruplex/Hemin to "switch-

on" the cathodic photocurrent of p-type PbS quantum dots: toward a versatile platform for photoelectrochemical aptasensing. *Anal. Chem.* **2015,** *87,* 2892-2900.
(42) Li, R.; Zhang, Y.; Tu, W.; Dai, Z. Photoelectrochemical bioanalysis platform for cells monitoring based on dual signal amplification using in situ generation of electron acceptor coupled with heterojunction. *ACS Appl. Mat. Interfaces* **2017,** *9,* 22289-22297.
(43) Huang, J.; Zhu, Y.; Yang, X.; Chen, W.; Zhou, Y.; Li, C. Flexible 3D porous CuO nanowire arrays for enzymeless glucose sensing: in situ engineered versus ex situ piled. *Nanoscale* **2015,** *7,* 559-569.
(44) Zhao, W.-W.; Xu, J.-J.; Chen, H.-Y. Photoelectrochemical enzymatic biosensors. *Biosens. Bioelectron.* **2017,** *92,* 294-304.
(45) Zhang, W. X.; Wen, X. G.; Yang, S. H.; Berta, Y.; Wang, Z. L. Single-crystalline scroll-type nanotube arrays of copper hydroxide synthesized at room temperature. *Adv. Mater.* **2003,** *15,* 822-825.
(46) Kim, D.-W.; Rhee, K.-Y.; Park, S.-J. Synthesis of activated carbon nanotube/copper oxide composites and their electrochemical performance. *J. Alloys Compd.* **2012,** *530,* 6-10.
(47) Reitz, J. B.; Solomon, E. I. Propylene oxidation on copper oxide surfaces: Electronic and geometric contributions to reactivity and selectivity. *J. Am. Chem. Soc.* **1998,** *120,* 11467-11478.
(48) Li, Z.; Xin, Y.; Zhang, Z. New photocathodic analysis platform with quasi-core/shell-structured TiO_2@Cu_2O for sensitive detection of H_2O_2 release from living cells. *Anal. Chem.* **2015,** *87,* 10491-10497.
(49) Pradhan, A. C.; Uyar, T. Morphological control of mesoporosity and nanoparticles within Co_3O_4-CuO electrospun nanofibers: Quantum confinement and visible light photocatalysis performance. *ACS Appl. Mat. Interfaces* **2017,** *9,* 35757-35774.
(50) Yang, M. Q.; He, J. H. Fine tuning of the morphology of copper oxide nanostructures and their application in ambient degradation of methylene blue. *J. Colloid Interface Sci.* **2011,** *355,* 15-22.
(51) Fishman, Z. S.; Rudshteyn, B.; He, Y. L.; Liu, B. L.; Chaudhuri, S.; Askerka, M.; Haller, G. L.; Batista, V. S.; Pfefferle, L. D. Fundamental role of oxygen stoichiometry in controlling the band gap and reactivity of cupric oxide nanosheets. *J. Am. Chem. Soc.* **2016,** *138,* 10978-10985.
(52) Zhao, W. W.; Ma, Z. Y.; Yan, D. Y.; Xu, J. J.; Chen, H. Y. In situ enzymatic ascorbic acid production as electron donor for CdS quantum dots equipped TiO_2 nanotubes: A general and efficient approach for new photoelectrochemical immunoassay. *Anal. Chem.* **2012,** *84,* 10518-10521.
(53) Zhu, Y.-C.; Zhang, N.; Ruan, Y.-F.; Zhao, W.-W.; Xu, J.-J.; Chen, H.-Y. Alkaline phosphatase tagged antibodies on gold nanoparticles/TiO_2 nanotubes electrode: A plasmonic strategy for label-free and amplified photoelectrochemical immunoassay. *Anal. Chem.* **2016,** *88,* 5626-5630.
(54) Tu, W.; Cao, H.; Zhang, L.; Bao, J.; Liu, X.; Dai, Z. Dual signal amplification using gold nanoparticles-enhanced zinc selenide nanoflakes and P19 protein for ultrasensitive photoelectrochemical biosensing of microRNA in cell. *Anal. Chem.* **2016,** *88,* 10459-10465.
(55) Zhang, L.; Ruan, Y.-F.; Liang, Y.-Y.; Zhao, W.-W.; Yu, X.-D.; Xu, J.-J.; Chen, H.-Y. Bismuth oxyiodide couples with glucose oxidase: A special synergized dual-catalysis mechanism for photoelectrochemical enzymatic bioanalysis. *ACS Appl. Mat. Interfaces* **2018,** *10,* 3372-3379.
(56) Huang, K.-J.; Niu, D.-J.; Sun, J.-Y.; Han, C.-H.; Wu, Z.-W.; Li, Y.-L.; Xiong, X.-Q. Novel electrochemical sensor based on functionalized graphene for simultaneous determination of adenine and guanine in DNA. *Colloids Surf., B* **2011,** *82,* 543-549.
(57) Yang, T.; Guan, Q.; Li, Q.; Meng, L.; Wang, L.; Liu, C.; Jiao, K. Large-area, three-dimensional interconnected graphene oxide intercalated with self-doped polyaniline nanofibers as a free-standing electrocatalytic platform for adenine and guanine. *J. Mater. Chem. B* **2013,** *1,* 2926-2933..

For TOC only